Can p,p′-Dimercaptoazobisbenzene Be Produced from p-Aminothiophenol by Surface Photochemistry Reaction in the Junctions of a Ag Nanoparticle–Molecule–Ag (or Au) Film?

ARTICLE *in* THE JOURNAL OF PHYSICAL CHEMISTRY C · SEPTEMBER 2010

Impact Factor: 4.77 · DOI: 10.1021/jp107305z

4 AUTHORS:

Yingzhou Huang
Chongqing University
37 PUBLICATIONS **850** CITATIONS
SEE PROFILE

Yurui Fang
Chalmers University of Technology
42 PUBLICATIONS **994** CITATIONS
SEE PROFILE

Zhilin Yang
Xiamen University
326 PUBLICATIONS **4,436** CITATIONS
SEE PROFILE

Mengtao Sun
Chinese Academy of Sciences
129 PUBLICATIONS **2,786** CITATIONS
SEE PROFILE

Can *p*,*p*′-Dimercaptoazobisbenzene Be Produced from *p*-Aminothiophenol by Surface Photochemistry Reaction in the Junctions of a Ag Nanoparticle−Molecule−Ag (or Au) Film?

Yingzhou Huang,[†,‡] Yurui Fang,[†] Zhilin Yang,[§] and Mengtao Sun*[,†]

Beijing National Laboratory for Condensed Matter Physics, Institute of Physics, Chinese Academy of Sciences, P.O. Box 603-146, Beijing 100190, Department of Applied Physics, Chongqing University, Chongqing 400044, and Department of Physics, Xiamen University, Xiamen 361005, People's Republic of China

Received: August 3, 2010; Revised Manuscript Received: September 11, 2010

In this study, we attempt to experimentally address the question of whether *p*,*p*′-dimercaptoazobisbenzene (DMAB) can be produced from *p*-aminothiophenol (PATP) by surface photochemistry reaction in the junctions of a Ag nanoparticle−molecule−Ag (or Au) film. First, utilizing surface-enhanced Raman scattering (SERS) spectra, we provide experimental and theoretical evidence that DMAB can be produced from PATP by surface photochemistry reaction in the junctions of a Ag nanoparticle−molecule−Ag film. Second, we investigate the SERS spectra utilizing both experimental and theoretical approaches, ultimately revealing that DMAB cannot be produced from PATP in the junctions of a Ag nanoparticle−molecule−Au film. The electromagnetic enhancements are estimated with three-dimensional finite-difference time domain methods, which are about 9×10^5 times in the junctions of Ag nanoparticle−PATP−Ag/Au films.

1. Introduction

Surface-enhanced Raman scattering (SERS) is widely used in chemistry, biology, physics, and material science because of its extremely high surface sensitivity and extensive applications of fingerprint vibrational spectroscopy in qualitative and quantitative analysis.[1,2] Currently, there are two kinds of enhancement mechanisms that are widely accepted. The first of these mechanisms is the electromagnetic (EM) enhancement,[1−4] which is caused by the strong surface plasmon resonance of curved metal surfaces coupled to incident light. The second of these mechanisms is the chemical enhancement,[5−7] which can be considered to be similar to a resonance Raman process between the ground electronic state of the molecule−metal complex and its new excited levels arising from charge transfer (CT) between the metallic surface and the adsorbed molecule.

Extensive experimental studies of the SERS of 4-aminothiophenol (PATP; see Figure 1a) adsorbed on different metal surfaces have, to date, been conducted.[8−18] The Raman peaks of PATP at 1140, 1390, and 1432 cm^{-1} on Ag nanoparticles can be clearly observed and are known as the "b_2 modes".[9] Recently, Wu and co-workers theoretically predicted that these vibrational modes come from the N═N related vibrations of *p*,*p*′-dimercaptoazobisbenzene (*trans*-DMAB; see Figure 1b) produced from PATP by catalytic coupling reaction on silver nanoparticles.[19] We not only provided experimental and theoretical evidence for this surface catalytic coupling reaction using time-dependent SERS spectra and density functional theory (DFT), but also revealed that these three Raman peaks of DMAB were strongly enhanced by plasmons (EM enhancement).[20] All of the enhanced vibrational modes in SERS spectra of DMAB were contributed by plasmons, not by the chemical enhancement mechanism, since all of these enhanced modes are the Ag group symmetry, not the Bu group symmetry.[20] Further experimental evidence has also been reported using surface mass spectroscopy and SERS measurements.[21] Whether such surface photochemistry reaction can occur on Ag or Au films is an interesting scientific issue.

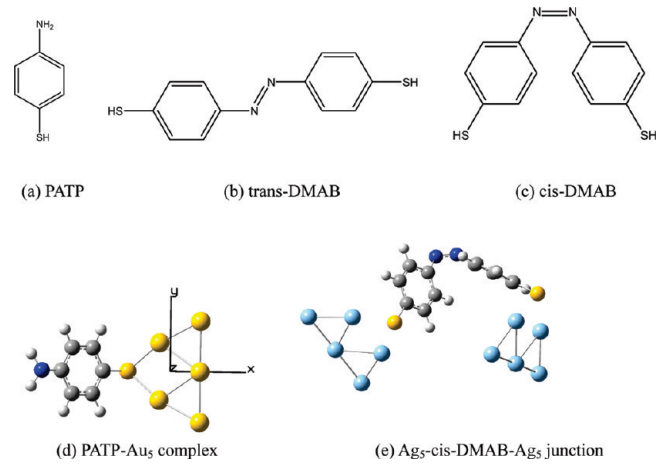

Figure 1. Molecular structures of (a) PATP, (b) *trans*-DMAB, and (c) *cis*-DMAB and theoretical models of the (d) PATP−Ag_5 complex and (e) Ag_5−*cis*-DMAB−Ag_5 junction.

To thoroughly address this problem, we adopted both a theoretical and an experimental approach. First, we measured the Raman spectra of PATP on Ag and Au films. Next, the Ag nanoparticles were attached to these two films and their Raman spectra measured using mapping methods. Then, their measured Raman peaks were identified via the quantum chemical method, a technique that is frequently used to examine whether DMAN has been produced. Finally, the electromagnetic enhancements were estimated using three-dimensional finite-difference time domain (3D-FDTD) methods. Through the combination of these

* To whom correspondence should be addressed. E-mail: mtsun@aphy.iphy.ac.cn.
† Chinese Academy of Sciences.
‡ Chongqing University.
§ Xiamen University.

10.1021/jp107305z
Published on Web 10/01/2010

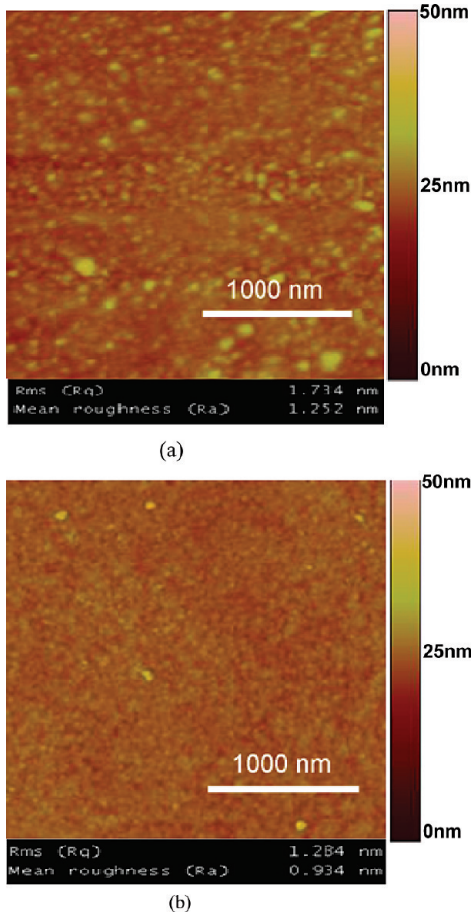

Figure 2. AFM images of the (a) Ag and (b) Au films.

techniques, we ultimately arrive at a reliable answer to the aforementioned question.

2. Experimental Section

PATP was purchased from Aldrich Chemical Co., which was used without further treatment or purification. The substrate for SERS measurement was prepared by evaporating Ag and Au metal onto silicon under a high vacuum using the electron beam evaporation system (model Peva-600E). The evaporation conditions were carefully controlled to produce a layer of Ag with an average thickness of 30 nm and a layer of Au with an average thickness of 100 nm. The surface roughness was evaluated with atomic force microscopy (AFM). These images (see Figure 2a,b) show that the roughness was 1.252 and 0.934 nm for the Ag and Au films, respectively. The Ag colloid was prepared with citrate reduction of $AgNO_3$ according to ref 22. $AgNO_3$ (90 mg) was dissolved in 650 mL of quartz distilled water. A 500 mL volume of this solution was brought to boiling, and then a solution of 1% sodium citrate (10 mL) was added. Thirty minutes later the remaining 150 mL of $AgNO_3$ solution was added three times every 15 min. The solution was boiled for about 1.5 h. To observe the size and the shape of the Ag nanoparticles, the scanning electron microscopy (SEM) image (see Figure 3a) was obtained using a field emission (FE) microscope (Sirion, FEI) operating at an accelerating voltage of 10 kV. The SEM figure (see Figure 3a) shows that most nanoparticles were nanospheres with an average diameter of 45 nm.

The Ag and Au films were immersed in a 5×10^{-6} M solution of PATP in ethanol for more than 5 h. The films were

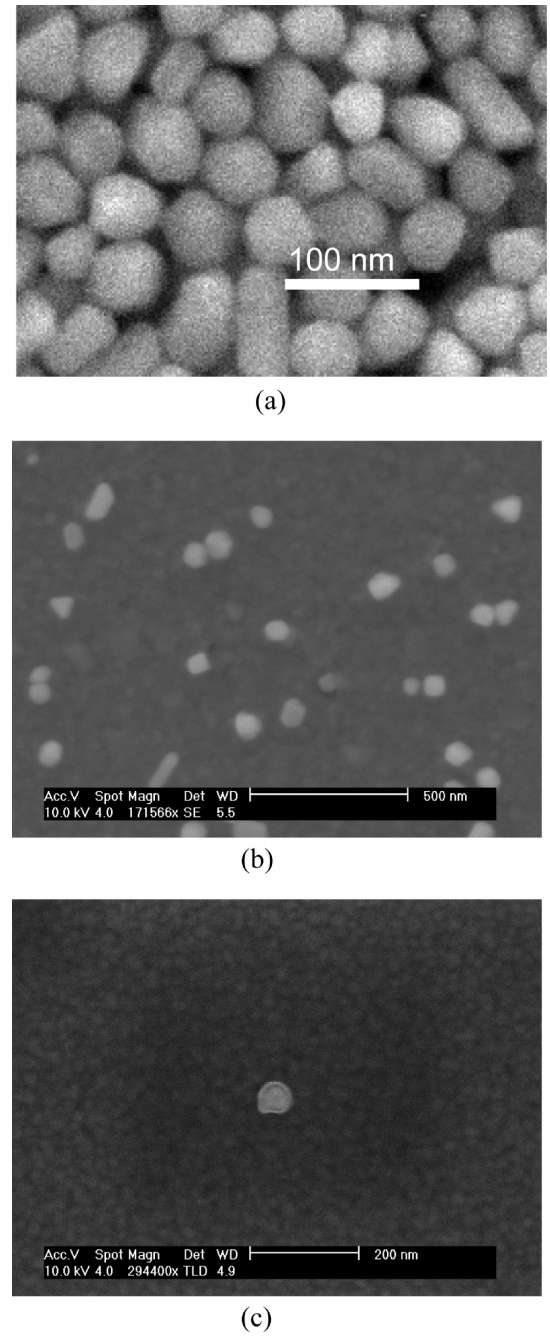

Figure 3. (a) SEM images of the Ag nanoparticles, (b) Ag nanoparticle−Ag film, and (c) Ag nanoparticle−Au film.

then washed in ethanol for 5 min. The Raman spectra of PATP on the Ag and Au films were measured with a Renishaw inVia Raman system equipped with an integral microscope (LEICA, DMLM). The 632.8 nm radiation from a 25 mW air-cooled argon ion laser was used as the excitation source. In our Raman experiment, the laser power irradiating the SERS sample was measured at 2 mW with a 50× objective. The appropriate holographic notch filter was placed in the spectrometer, and the holographic grating (1800 grooves/mm) and slit installed in the spectrometer produced a spectral resolution of 1 cm^{-1} with a repeatability of $\leq \pm 0.2$ cm^{-1}. Raman scattering was detected using a Peltier-cooled CCD detector (576 × 384 pixels). The data acquisition time used in the experiment was 10 s.

The PATP−Ag film and PATP−Au film were immersed into the 5-fold diluted Ag colloid solution for 1 h. After that, the films were gently rinsed with deionized water several times.

The surface morphology was characterized by SEM with energy-dispersive spectroscopy (Hitachi S-4800). Figure 3 shows the SEM images of the junctions of the Ag nanoparticle−molecule−Ag/Au films. Their Raman spectra were then measured by scanning a 30 × 30 μm area. Other experimental methods and processes are the same as those mentioned above.

3. Theoretical Methods

The photoisomers of *trans*-DMAB and *cis*-DMAB can be seen in parts b and c, respectively, of Figure 1. The models of the PATP−Au_5 complex (see Figure 1d) and the Ag_5−*cis*-DMAB−Ag_5 junction (see in Figure 1e) were employed to simulate the SERS spectra of PATP on the Au film and DMAB on the Ag film. Their ground-state geometries were optimized using density functional theory (DFT),[23] the PW91PW91 functional,[24] the 6-31G(d) basis set for C, H, S, and N, and the LANL2DZ basis set[25] for Ag and Au. Their SERS spectra were simulated with optimized ground-state geometry, using the same functional and basis set. The optical absorption of the PATP−Au_5 complex was calculated using time-dependent DFT (TD-DFT),[26] the LC-PW91PW91 functional, the 6-31G(d) basis set for C, H, S, and N, and the LANL2DZ basis set for Ag and Au. It is noted that the long-range (LC) related density functional[27] was employed in the optical absorption calculations. The ground-state geometry of isolated *cis*-DMAB was optimized with DFT, the PW91PW91 functional, and the 6-31G(d) basis set. The electronic transitions of isolated DMAB were calculated with TD-DFT, the PW91PW91 functional, and the 6-31G(d) basis set. All the quantum chemical calculations were performed with the Gaussian 09 suite.[28] The orientation of charge transfer on electronic transitions was visualized using the charge difference density.[7]

The local electromagnetic enhancement in the junctions of the Ag nanoparticle−Ag/Au films was calculated using the FDTD method.[29] All FDTD calculations were conducted in the platform of a commercial XFDTD software package (RemCom XFDTD 6.3). In this work, we adopted the general Drude model to simulate the complex permittivity of Au and Ag using the form[30−32]

$$\varepsilon(\omega) = \varepsilon_\infty + \frac{\varepsilon_s - \varepsilon_\infty}{1 + i\omega\tau} + \frac{\sigma}{i\omega\varepsilon_0} \quad (1)$$

where ε_s, ε_∞, σ, τ, ω, and ε_0 represent the static permittivity, infinite frequency permittivity, conductivity, relaxation time, angular frequency, and permittivity of free space, respectively. The four parameters ε_s, ε_∞, σ, and τ can be adjusted through curve-fitting techniques to correctly match the complex permittivity, which can be derived from the experimentally determined optical constants. The number of periods of the incident sinusoidal plane wave was set to 12 to guarantee calculation convergence, which could be judged by checking whether near-zone electric field values had reached the steady state. The amplitude of the sinusoidal plane wave was set to be 1 V/m in the calculation.

4. Results and Discussion

It is found that a weak SERS signal was observed on the Ag film while an SERS signal could not be observed on the Au film at all (see Figure 4a,b). To significantly increase the Raman signals and judge whether DMAB can be produced on the Au film, Ag nanoparticles were deposited onto the functionalized Ag and Au. Next, their Raman spectra were measured by scanning a 30 × 30 μm area. Here, we found that when the laser light was not focused on one of the junctions of the Ag nanoparticle−molecule−Ag/Au films, the resulting SERS spectra were similar to those measured on the PATP−Ag/Au films. Conversely, when the junctions of the Ag nanoparticle−molecule−Ag/Au films were illuminated, their Raman spectra were significantly enhanced (Figure 4c,d).

In comparing parts a and c of Figure 4, we noticed that the profiles of the Raman spectra were quite similar, but the Raman signals were strongly enhanced by electromagnetic fields due to the coupling between the Ag nanoparticles and the Ag film. The FDTD calculations (Figure 5a) revealed that the Raman signal could be enhanced by a factor of 9.22×10^5 when illuminated with 632.8 nm light, which is estimated using the relation $|M|^4 = |E_{loc}|^4/|E_{in}|^4$, where E_{loc} and E_{in} are the local and incident electric fields, respectively. It should be noted that the k of the electric field is perpendicular to the surface, so the SERS enhancement $|M|^4$ is not as strong as the enhancement in tip-enhanced Raman scattering (TERS),[33,34] where the angle between k and the surface is 60°. It is found that the strongest enhancement (see Figure 5) is not at the center of the gap (the gap distance in the calculation is 1 nm). The two strongest electromagnetic enhancements appear near the gap (shifted several nanometers along the film, compared to the gap center).

Our previous study[20] showed that the strong peaks at 1390 and 1432 cm^{-1} are related to the N═N vibration of the *trans*-DMAB vibrational modes (see Figure 4e). Thus, parts a and c of Figure 4 provide experimental evidence that DMAB can be produced from PATP by surface photochemistry reaction on the Ag film and in the junctions of the Ag nanoparticle−molecule−Ag film. In the junction of the Ag_5−*trans*-DMAB−Ag_5 system, our previous theoretical results[20] reveal that chemical enhancements, including static chemical enhancement and resonant effects on electronic transitions, are on the order of 10^3. Only the model of the Ag_5−*trans*-DMAB−Ag_5 junction was examined in our previous theoretical study.[20] In this study, we simulated the Raman spectrum of Ag_5−*cis*-DMAB−Ag_5 junctions (see Figure 4g), since this is also a possible adsorbed model.[35] It was found that the SERS spectrum using this model cannot reproduce the experimental data in Figure 4c. Therefore, from these two studies we can safely conclude that the SERS spectra of DMAB can be reproduced by the Ag_5−*trans*-DMAB−Ag_5 junction model and not by the model of the Ag_5−*cis*-DMAB−Ag_5 junction.

The electronic structure of isolated *trans*-DMAB has been theoretically examined in our previous study.[20] With the same method, the electronic structure of isolated *cis*-DMAB is examined at the same level of theory in this study. The calculated transition energies and oscillator strengths can be seen in Table 1. The C−N═N−C dihedral angle is 14.04°. The orientation of charge transfer can be seen in Figure 6. Here, it is found that the S_1 excited state of *trans*-DMAB is dark absorption, while for *cis*-DMAB we see strong absorption at 574 nm. A strong absorption of this nature is not seen in the time-dependent extinction spectra of PATP in Ag sol (see Figure 2 in ref 20). This is, thus, further evidence that *cis*-DMAB is not the correct model to be applied to our system of study.

Since the Raman spectrum of the molecule of interest cannot be clearly observed on the Au film, it is hard to judge whether DMAB can be produced on the Au film (see Figure 4b). To significantly increase the Raman signal strength, Ag nanoparticles were deposited onto functionalized Au films. Next, their Raman spectra were measured by scanning over a 30 × 30 μm area. When the laser light is focused on the junctions of the Ag

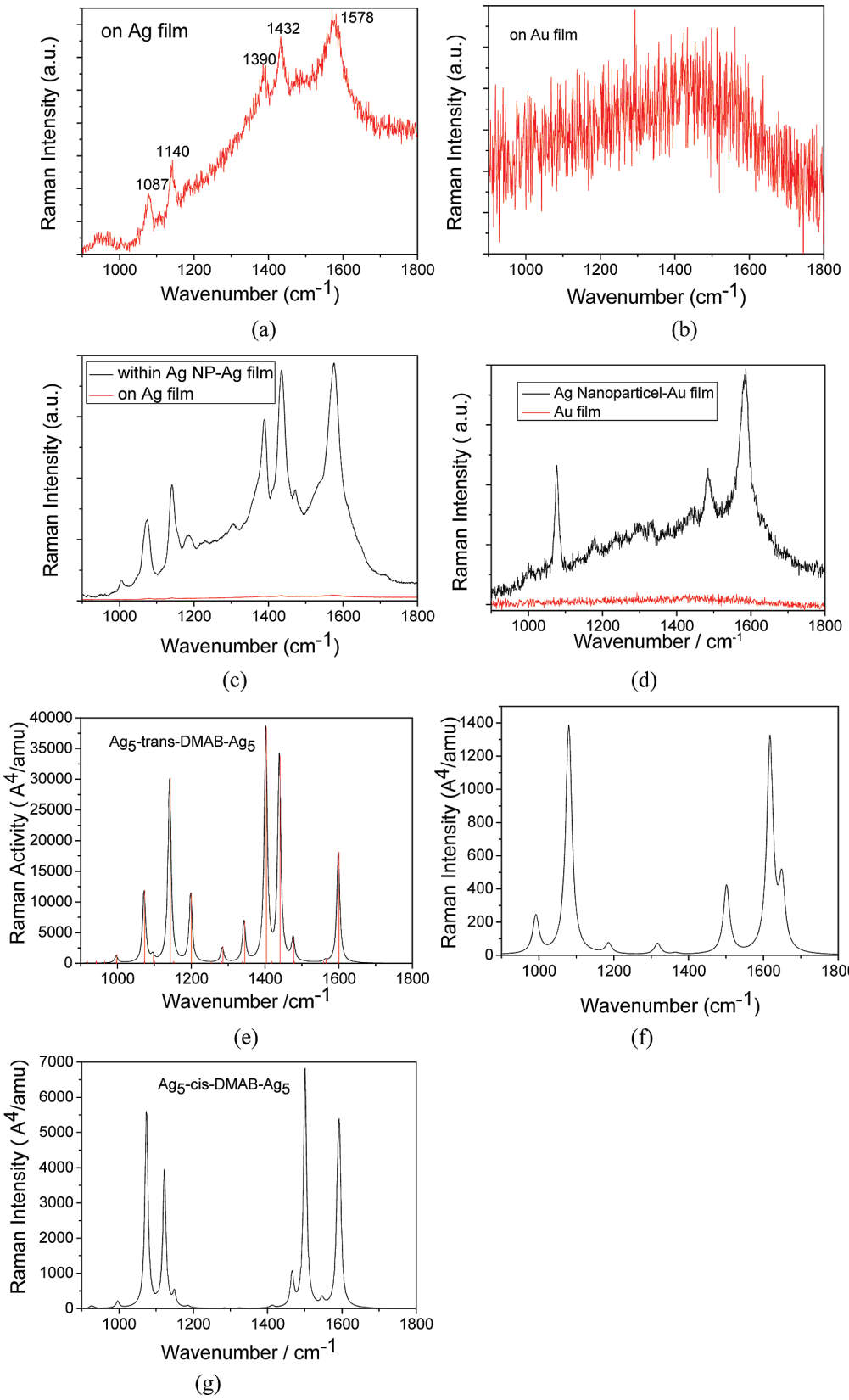

Figure 4. Raman spectra of a molecule (a) on the Ag film, (b) on the Au film, (c) in the junctions of the Ag nanoparticle−Ag film, and (d) in the junctions of the Ag nanoparticle−Au film. SERS spectra of (e) the Ag_5−*trans*-DMAB−Ag_5 junction, (f) the PATP−Au_5 complex, and (g) the Ag_5−*cis*-DMAB−Ag_5 junction. Panel e is reprinted from ref 20. Copyright 2010 American Chemical Society.

nanoparticle−molecule−Au film, the Raman signal is significantly enhanced and can be clearly observed (Figure 4d). This effect is attributed to the electromagnetic enhancement due to the coupling of the Ag nanoparticles and the Au film. FDTD simulations (Figure 5a) show that the SERS enhancement ($|M_{junction}|^4$) is 9.05×10^5 at the junction of the Ag nanoparticle−molecule−Au film when illuminated with 632.8 nm incident radiation.

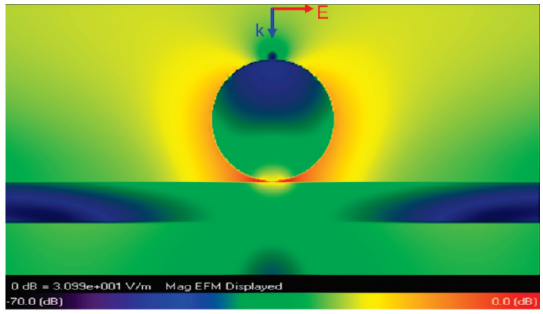

(A)

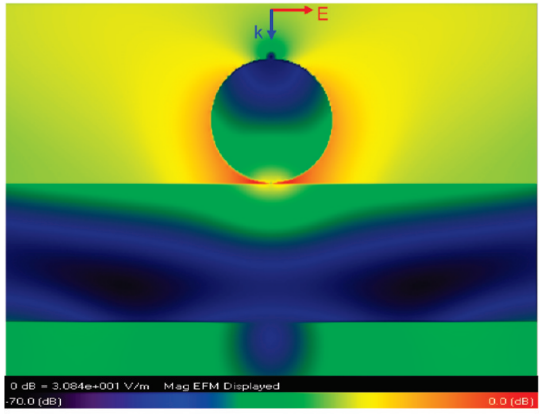

(B)

Figure 5. (a) Local electric field distribution of the Ag nanoparticle and Ag film, where the diameter of the Ag nanoparticle is 90 nm and the thickness of the Ag film is 30 nm. (b) Local electric field distribution of the Ag nanoparticle and Au film, where the diameter of the Ag nanoparticle is 90 nm and the thickness of the Au film is 100 nm. The color bar is shown at the bottom of the panels.

TABLE 1: Electronic Transitions of *cis*-DMAB

trans-DMAB[a]	*cis*-DMAB
$1B_g$, 560.29 nm, $f = 0.0000$	A_1, 573.99 nm, $f = 0.1272$
^1B_u, 448.40 nm, $f = 1.1945$	A_2, 415.96 nm, $f = 0.1256$

[a] The data were taken from ref 20.

It is found that the profiles of the Raman spectra of the molecule in the Ag nanoparticle−molecule−Ag film and those of the Ag nanoparticle−PATP−Au film differ significantly. The simulated Raman spectrum (see Figure 4f) of the PATP−Au_5 complex (where S of PATP is adsorbed on the Au_5 cluster) is consistent with the experimental result for the Ag nanoparticle−PATP−Au film, which reveals that DMAB cannot be produced from PATP in the junctions of the Ag nanoparticle−molecule−Au film. The chemical enhancement of PATP on the Au film is a factor of 60, compared with the intensity of the vibrational mode at 1078 cm^{-1} of isolated PATP (the Raman intensity is 1384 A^4/amu for the PATP−Au_5 complex). To study the possible resonance effect on the Raman signal at the junctions of the Ag nanoparticle−molecule−Au film, electronic transitions of the PATP−Au_5 complex were calculated (see the data in Table 2). Here, it was found that the lowest optical absorption was at 374 nm, revealing that there is no resonance effect in our experiment with incident light of 632.8 nm. Thus, the chemical enhancement arises from the static charge transfer at the ground state due to the interaction between PATP and the metal. Theoretical calculations demonstrate that 0.025 e is transferred to PATP from the Au_5 cluster. The charge transfer between the molecule and the clusters results in an increase in the electronic static polarizability (see the data in Table 3), which then results in the chemical enhancement of the SERS signal.

TABLE 2: Electronic Transitions of the PATP−Au_5 Complex

S_1	373.83 nm, $f = 0.0235$
S_2	341.08 nm, $f = 0.1534$
S_3	318.06 nm, $f = 0.0054$
S_4	317.58 nm, $f = 0.2197$
S_5	310.70 nm, $f = 0.0888$
S_6	296.85 nm, $f = 0.0054$

TABLE 3: Calculated Static Electronic Polarizabilities (au) of the PATP−Au_5 Complex

xx	*yy*	*zz*
429.976	333.894	183.345

The adsorption and reaction mechanisms of a molecule adsorbed on Ag and Au films, in Ag nanoparticle−molecule−Ag/Au films, can be seen in Figures 7 and 8. First, DMAB produced on the Ag film by surface photochemistry reaction and the Raman signal of DMAB, due to large chemical enhancement, can be observed in Figure 4a. There may be two forms (*trans* and *cis* forms) of DMAB adsorbed on the Ag film (see Figure 6). Second, the Ag nanoparticles were deposited on the Ag film onto which the DMAB was adsorbed. As a result, stronger Raman signals of DMAB (see Figure 4c) were observed due to the enormous electromagnetic enhancement (a factor of 9.22×10^5) arising from the coupling between the Ag nanoparticles and the Ag film. The SERS spectrum of DMAB was reproduced by the model of the Ag_5−*trans*-DMAB−Ag_5 junction and, conversely, not by the model of the Ag_5−*cis*-DMAB−Ag_5 junction.

For the second case, PATP adsorbed on the Au film, no Raman signal was observed (see Figure 4b) due to the fact that

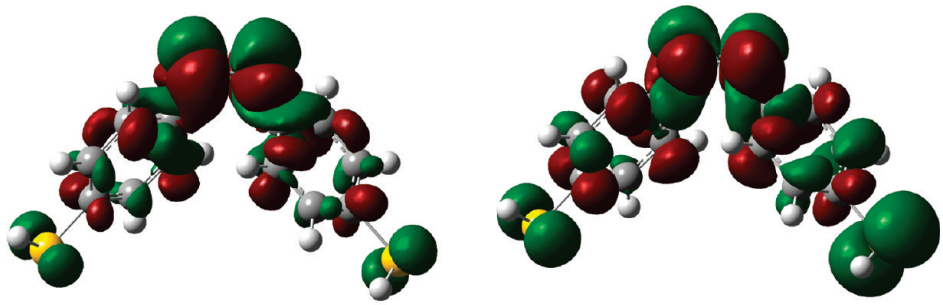

S_1 S_2

Figure 6. Charge difference density of *cis*-DMAB, where green and red stand for the hole and electron, respectively.

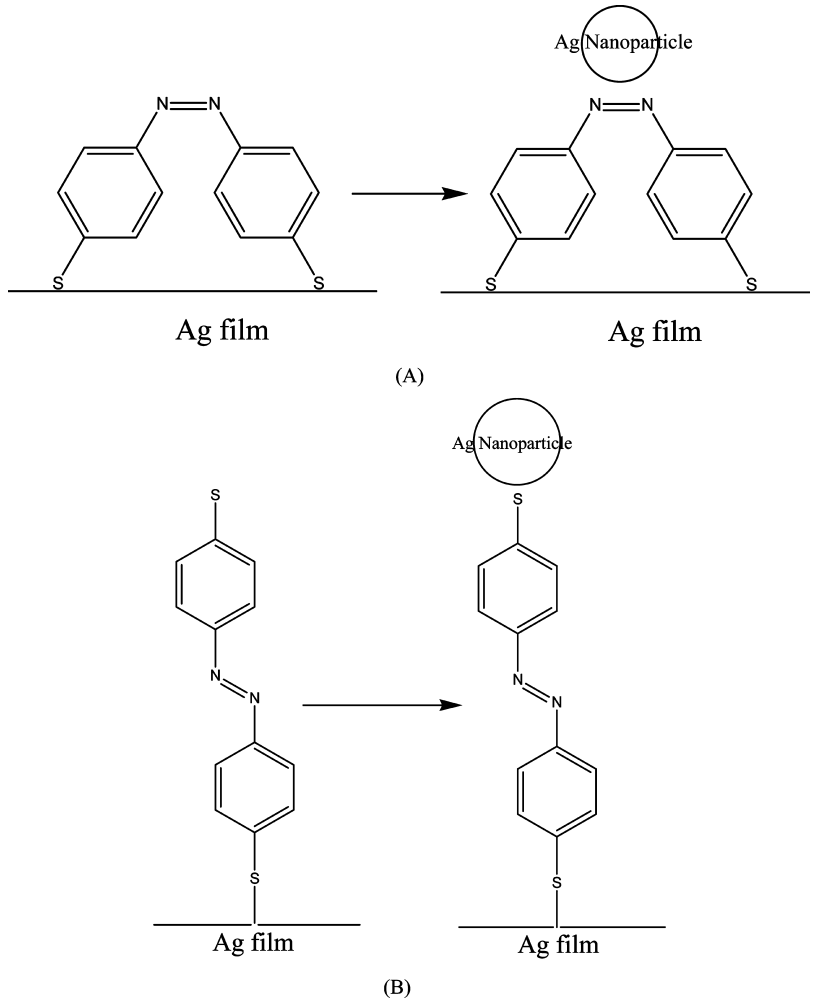

Figure 7. Mechanism of a molecule adsorbed on the Ag film, (a) *cis*-DMAB film, and (b) *trans*-DMAB−Ag film.

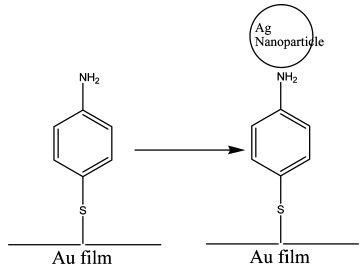

Figure 8. Mechanism of a molecule adsorbed on the Au film.

the chemical enhancement is weak (only a factor of 60). The Ag nanoparticles were deposited on the Au film onto which PATP was adsorbed, and a stronger PATP Raman signal (see Figure 4d) was observed due to the enormous electromagnetic enhancement (a factor of 9.05×10^5) arising from the coupling between the Ag nanoparticles and the Au film.

It is found that the electromagnetic enhancements for these two junctions are almost the same while their chemical enhancements are quite different. On the Ag film, the chemical enhancement is on the order of 10^3; however, on the Au film, the chemical enhancement is only a factor of 60. We also can conclude that the Ag nanoparticle on the Ag/Au film only plays a role in the electromagnetic enhancement through the coupling between the Ag nanoparticles and the Ag/Au films, which do not play roles in the surface photochemistry reaction.

It is important to reveal the reason that DMAB can be produced from PATP by surface photochemistry reaction in the junction of the Ag nanoparticle−molecule−Ag film while it cannot be produced in the junction of the Ag nanoparticle−molecule−Au film. Our understanding is the collective oscillation of the free electrons at the Ag metal−dielectric interface is much stronger than that from the Au surface, or the oxidation potential of Au is significantly higher than that of Ag.

5. Conclusion

Experimental and theoretical results revealed that DMAB can be produced from PATP by surface photochemistry reaction in the junctions of the Ag nanoparticle−molecule−Ag film, but cannot be produced from PATP by surface photochemistry reaction at the junctions of the Ag nanoparticle−molecule−Au film. The electromagnetic enhancement in the junctions of the Ag and Au nanoparticle−molecule−Ag films are on the order of 9×10^5. The chemical enhancement on the Au film was measured to be a factor of 60, providing no resonance effect with respect to the SERS enhancement.

Acknowledgment. This work was supported by the National Natural Science Foundation of China (Grant Nos. 10874234, 20703064, and 90923003) and the National Basic Research Project of China (Grant No. 2009CB930701). We thank Xiaorui Tian, who prepared the Ag and Au films, using the electron beam evaporation system at the Laboratory of Microfabrication, Institute of Physics, Chinese Academy of Sciences.

References and Notes

(1) Moskovits, M. *Rev. Mod. Phys.* **1985**, *57*, 783.

(2) Xu, H. X.; Bjerneld, E. J.; Kail, M.; Borjesson, L. *Phys. Rev. Lett.* **1999**, *83*, 4357.
(3) Metiu, H.; Dos, P. *Annu. Rev. Phys. Chem.* **1984**, *35*, 507.
(4) Kneipp, K.; Kneipp, H.; Itzkan, I.; Dasari, R. R.; Feld, M. S. *Chem. Rev.* **1999**, *99*, 2957.
(5) Otto, A. *J. Raman Spectrosc.* **2005**, *36*, 497.
(6) Lombardi, J. R.; Birke, R. L. *J. Phys. Chem. C* **2008**, *112*, 5605.
(7) Sun, M. T.; Liu, S.; Chen, M.; Xu, H. X. *J. Raman Spectrosc.* **2009**, *40*, 137.
(8) Hill, W.; Wehling, B. *J. Phys. Chem.* **1993**, *97*, 9451.
(9) Osawa, M.; Matsuda, N.; Yoshii, K.; Uchida, I. *J. Phys. Chem.* **1994**, *98*, 12702.
(10) Wang, J.; Zhu, T.; Fan, Z. F. *Acta Phys. Chem.* **1998**, *94*, 485.
(11) Cao, L.; Diao, P.; Tong, L.; Zhu, T.; Liu, Z. F. *ChemPhysChem* **2005**, *6*, 913.
(12) Gibson, J. W.; Johnson, B. R. *J. Chem. Phys.* **2006**, *124*, 064701.
(13) Fromm, D. P.; Sundaramurthy, A.; Kinkhabwala, A.; Schuck, P. J.; Kino, G. S.; Moerner, W. E. *J. Chem. Phys.* **2006**, *124*, 061101.
(14) Baia, M.; Toderas, F.; Baia, L.; Popp, J.; Astilean, S. *Chem. Phys. Lett.* **2006**, *422*, 127.
(15) Zhou, Q.; Li, X. W.; Fan, Q.; Zhang, X. X.; Zheng, J. W. *Angew. Chem., Int. Ed.* **2006**, *45*, 3970.
(16) Zhou, Q.; Zhao, G.; Chao, Y. W.; Li, Y.; Wu, Y.; Zheng, J. W. *J. Phys. Chem. C* **2007**, *111*, 1951.
(17) Toderas, F.; Baia, M.; Baia, L.; Astilean, S. *Nanotechnology* **2007**, *18*, 255702.
(18) Wang, Y. L.; Zou, X Q.; Ren, W.; Wang, W. D.; Wang, E. K. *J. Phys. Chem. C* **2007**, *111*, 3259.
(19) Wu, D. Y.; Liu, X. M.; Huang, Y. F.; Ren, B.; Xu, X.; Tian, Z. Q. *J. Phys. Chem. C* **2009**, *113*, 18212.
(20) Fang, Y. R.; Li, Y. Z.; Xu, H. X.; Sun, M. T. *Langmuir* **2010**, *26*, 7737.
(21) Huang, Y. F.; Zhu, H. P.; Liu, G. K.; Wu, D. Y.; Ren, B.; Tian, Z. Q. *J. Am. Chem. Soc.* **2010**, *132*, 9301.
(22) Lee, P. C.; Meisel, D. *J. Phys. Chem.* **1982**, *86*, 3391.
(23) Hohenberg, P.; Kohn, W. *Phys. Rev.* **1964**, *136*, B864.
(24) Perdew, J. P.; Burke, K.; Wang, Y. *Phys. Rev. B* **1996**, *54*, 16533.
(25) Hay, P. J.; Wadt, W. R. *J. Chem. Phys.* **1985**, *82*, 270.
(26) Gross, E. K. U.; Kohn, W. *Phys. Rev. Lett.* **1985**, *55*, 2850.
(27) Drew, A.; Head-Gordon, M. *J. Am. Chem. Soc.* **2004**, *126*, 4007.
(28) Frisch, M. J.; Trucks, G. W.; Schlegel, H. B.; Scuseria, G. E.; Robb, M. A.; Cheeseman, J. R.; Scalmani, G.; Barone, V., Mennucci, B.; Petersson, G. A.; Nakatsuji, H.; Caricato, M.; Li, X.; Hratchian, H. P.; Izmaylov, A. F.; Bloino, J.; Zheng, G.; Sonnenberg, J. L.; Hada, M.; Ehara, M.; Toyota, K.; Fukuda, R.; Hasegawa, J.; Ishida, M.; Nakajima, T.; Honda, Y.; Kitao, O.; Nakai, H.; Vreven, T.; Montgomery, J. A.; Peralta, J. E., Jr.; Ogliaro, F.; Bearpark, M.; Heyd, J. J.; Brothers, E.; Kudin, K. N.; Staroverov, V. N.; Kobayashi, R.; Normand, J.; Raghavachari, K.; Rendell, A.; Burant, J. C.; Iyengar, S. S.; Tomasi, J.; Cossi, M.; Rega, N.; Millam, J. M.; Klene, M.; Knox, J. E.; Cross, J. B.; Bakken, V.; Adamo, C.; Jaramillo, J.; Gomperts, R.; Stratmann, R. E.; Yazyev, O.; Austin, A. J.; Cammi, R.; Pomelli, C.; Ochterski, J. W.; Martin, R. L.; Morokuma, K.; Zakrzewski, V. G.; Voth, G. A.; Salvador, P.; Dannenberg, J. J.; Dapprich, S.; Daniels, A. D.; Farkas, O.; Foresman, J. B.; Ortiz, J. V.; Cioslowski, J.; Fox, D. J. *Gaussian 09*, revision A.02; Gaussian, Inc.: Wallingford, CT, 2009.
(29) Kunz, K. S.; Luebber, R. J. *The Finite Difference Time Domain Method for Electromagnetics*; CRC: Cleveland, OH, 1993.
(30) Etchegoin, P. G.; Le Ru, E. C.; Meyer, M. *J. Chem. Phys.* **2006**, *125*, 164705.
(31) Hao, F.; Nordlander, P. *Chem. Phys. Lett.* **2007**, *446*, 115.
(32) Krug, J. T.; IJ. Sanchez, I. E.; Xie, X. S. *J. Chem. Phys.* **2002**, *116*, 10895.
(33) Yang, Z.; Aizpurua, J.; Xu, H. X. *J. Raman Spectrosc.* **2009**, *40*, 1343.
(34) Sun, M. T.; Fang, Y.; Yang, Z.; Xu, H. X. *Phys. Chem. Chem. Phys.* **2009**, *11*, 9412.
(35) Turansky, R.; Konpka, M.; Doltsinis, N. L.; Stich, I.; Marx, D. *ChemPhysChem* **2010**, *11*, 345.

JP107305Z